Extracting subnanometer single shells from ultralong multiwalled carbon nanotubes

Byung Hee Hong*, Joshua P. Small*, Meninder S. Purewal*, Asher Mullokandov*, Matthew Y. Sfeir*, Feng Wang*, Ju Young Lee†, Tony F. Heinz*, Louis E. Brus*, Philip Kim*‡, and Kwang S. Kim†‡

*Nanoscale Science and Engineering Center, Columbia University, New York, NY 10027; and †National Creative Research Initiative Center for Superfunctional Materials, Department of Chemistry, Division of Molecular and Life Sciences, Pohang University of Science and Technology, Pohang 790-784, Korea

Edited by Charles M. Lieber, Harvard University, Cambridge, MA, and approved August 25, 2005 (received for review June 22, 2005)

We report a simple but powerful method for engineering multiwalled carbon nanotubes (MWNTs) by using manipulation by an atomic-force microscope. The successive shell-by-shell extraction process of ultralong MWNTs allows the exposure of the innermost single-walled carbon nanotubes (SWNTs), which have diameters as small as ≈0.4 nm. The inner-shell extraction process changes the electrical characteristics of the MWNTs. Whereas the outer hollowed-out nanotubes show either metallic or semiconducting character, the innermost SWNTs of small diameter exhibit predominantly metallic transport properties.

atomic-force microscope | double-walled carbon nanotube | extraction | single-walled carbon nanotube | resonance Raman spectroscopy

Multiwalled carbon nanotubes (MWNTs) (1) exhibit high ductility with extremely high tensile strength (2). These properties have enabled a variety of mechanical manipulations of these structures (2–6), as well as possible device applications. Engineering the MWNT shell structure further permits controlled modification of the electrical properties (7, 8). Moreover, MWNTs are composed of strong, single-walled carbon nanotube (SWNT) shells coupled only by weak van der Waals interactions (9) associated with the nonlocal nature of the π–π dispersion forces (10). This situation results in ultralow friction between shell layers (9, 11) and leads to the possibility of nanoscale engineering of MWNT structures by displacing the shells with respect to one another. Such striking manipulations have indeed been realized in earlier investigations (11, 12) in which a group of inner shells was extended by a few micrometers (8) in a transmission electron microscope chamber after electrical vaporization of MWNT end caps. Potential applications of these MWNT structures, such as nanobearings (11) and nanooscillators (13, 14), have been suggested. In the present work, we introduce a simple and highly flexible approach based on standard atomic-force microscope (AFM) techniques that yields extensions over distances of several hundreds of micrometers. This method achieves controlled shell-by-shell extraction down to the innermost SWNT without chemical (15, 16) or electrical (11, 12) modification of the outer shells.

Methods

The essence of the extraction method of inner shells from MWNTs can be understood from Fig. 1*A*. The image shows the result of moving an AFM tip along the substrate perpendicular to the axis of a long MWNT at a rate of 0.5–0.8 cm/s. The height profile along the resulting structure (Fig. 1*B*) shows that the nanotube diameter drops in a stepwise fashion, corresponding to the successive extraction of the inner shells. We understand the nanotube extraction process as follows. As the length of MWNT segment displaced by the AFM tip increases, the total force required to overcome the friction of moving the MWNT across the substrate increases. The outer shell of the MWNT is subject to rupture when the force applied by the AFM tip exceeds its critical tensile strength (≈10–100 GPa) (2). As the motion of the AFM tip continues, the extruded inner shells are subject to the next stage of extraction (Fig. 1*A Inset*) after breaking the outer walls. In the case of SWNTs, similar manipulation simply leads to breaking upon extension (17). The length of the next stage of the extracted nanotube structure can be influenced by control of the AFM scan. If the extracted nanotube comes into contact with the substrate, it will rupture in a fashion analogous to that just described for the initial extraction step. However, a much greater

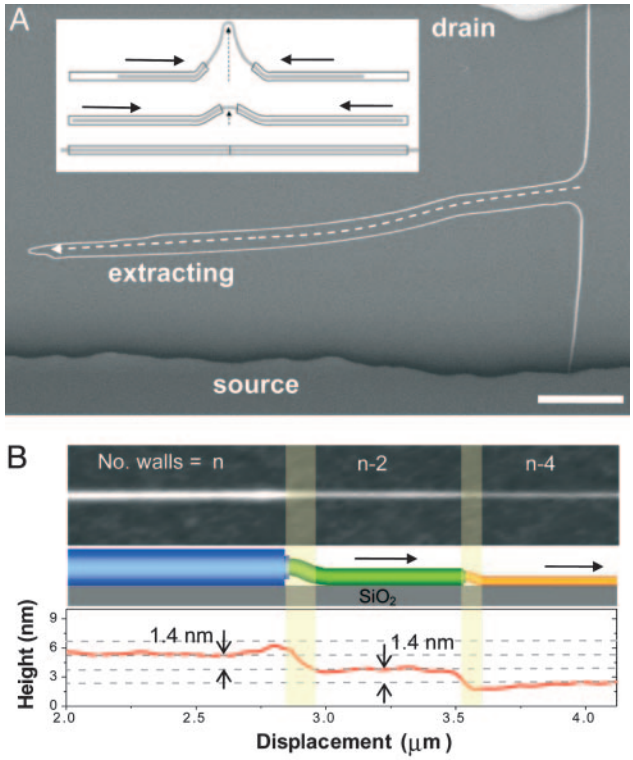

Fig. 1. Scanning electron microscope (SEM)/AFM images and a height profile showing the extraction process of MWNTs. (*A*) A SEM image of a manipulated MWNT formed by moving the AFM tip perpendicular to the nanotube axis. *Inset* illustrates schematically how the AFM tip breaks the outermost shells and causes the extrusion of the inner shells of the MWNT. (Scale bar: 10 μm.) (*B*) An AFM height profile showing the stepwise decrease of the diameter along the extracted nanotube. The illustration shows the extraction process. Each successive structure corresponds to a decrease of the hollowed-out nanotube by two shells.

This paper was submitted directly (Track II) to the PNAS office.

Abbreviations: MWNT, multi-walled carbon nanotube; AFM, atomic-force microscope; SWNT, single-walled carbon nanotube; SEM, scanning electron microscope.

‡To whom correspondence may be addressed. E-mail: pkim@phys.columbia.edu or kim@postech.ac.kr.

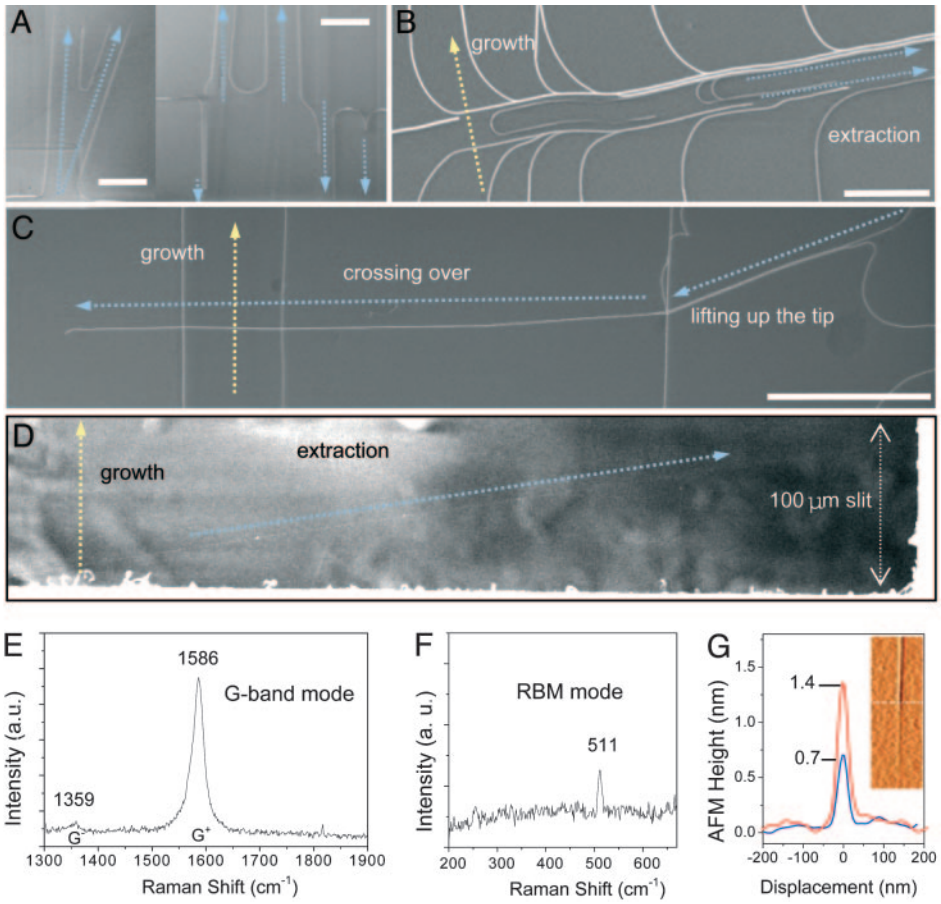

Fig. 2. SEM images, Raman spectra, and AFM profiles illustrating the formation of complex patterns of nanotubes, as well as the extraction of the innermost SWNTs with subnanometer diameter. (*A*) SEM images of nanotube patterns formed by multiple extractions in different directions. (Scale bars: 2 μm.) (*B*) SEM images of nanotube patterns produced by AFM manipulation of the initial MWNT. (Scale bar: 10 μm.) (*C*) A SEM image of nanotube interconnections created by the ''flying-tip'' extraction scheme. (Scale bar: 50 μm.) (*D*) A SEM image of an extracted nanotube suspended across a 100-μm-wide slit in a silicon substrate. The extraction direction is perpendicular to the growth direction of the MWNT. (*E* and *F*) The G band and radial breathing mode peaks in the Raman spectra observed in *D*. (*G*) An AFM profile showing the thinnest diameter of extracted SWNTs of ≈0.4 nm. *Inset* is the corresponding AFM image, where the step in the height is marked with a dotted line.

extension of the inner shells is possible if the AFM guides the nanotube above the surface, thus eliminating friction with the substrate.

The growth of ultralong MWNTs is an important ingredient in achieving controlled successive shell extraction. In contrast to the well established growth methods for SWNTs (18–20), the synthesis of long MWNTs has remained less developed. We have recently succeeded in growing ultralong MWNTs (>10 cm) on substrates by chemical vapor deposition. Through suitable control of the size of the Fe catalyst along with flow rate and temperature, we have produced centimeter-long MWNTs with diameters of 1.5–20 nm.

Results and Discussion

The AFM line traces along the extruded MWNT typically exhibit diameters decreased by steps of ≈1.4 nm, as shown in the representative data of Fig. 1. The change in diameter corresponds to approximately four times the intershell spacing (≈0.35 nm) in MWNTs. This change indicates that the extraction process leaves behind hollowed-out nanotubes consisting of pairs of shells. Single-shell steps (≈0.7 nm) were also observed, but the extracted plateaus were short (<100 nm) compared with those of double-shell steps (>500 nm). We attribute the preference for producing double-shell structures after extrusion to an enhancement of the friction between the two outermost nanotubes associated with a surface-induced deformation of the outer shell (21). After the consecutive removal of pairs of shells from a MWNT, the structure remaining in the last extraction step is either a SWNT or double-walled nanotube (DWNT). In the case of a residual DWNT, we find that it is still possible to extract the innermost SWNT from this structure.

Because the MWNT extraction procedure can be repeated as long as inner shells are present, we can reinitiate the process at different locations and in different directions by using newly exposed MWNT shells (Fig. 2*A*). Complicated patterns of MWNT shells can consequently be constructed (Fig. 2*B*). Moreover, the extracted nanotubes are attached to the AFM tip and can, if desired, be moved above the surface. This property permits us to form large-scale interconnects with neighboring nanotubes (Fig. 2*C*). We also used this technique to produce extracted shells that could be freely suspended across narrow slits in the substrate (Fig. 2*D*).

To investigate the diameter of the innermost shells, we applied Raman spectroscopy (22) to a thin extruded nanotube prepared in the configuration of Fig. 2*D*. Fig. 2 *E* and *F* show the Raman intensities of the G band and radial breathing mode (RBM). The high frequency (511 cm^{-1}) of the RBM peak and the large splitting between the G^+ and G^- modes imply a SWNT with a diameter of 0.40 nm (23). On the basis of the RBM frequency and the presence of an electronic resonance for the 514-nm laser

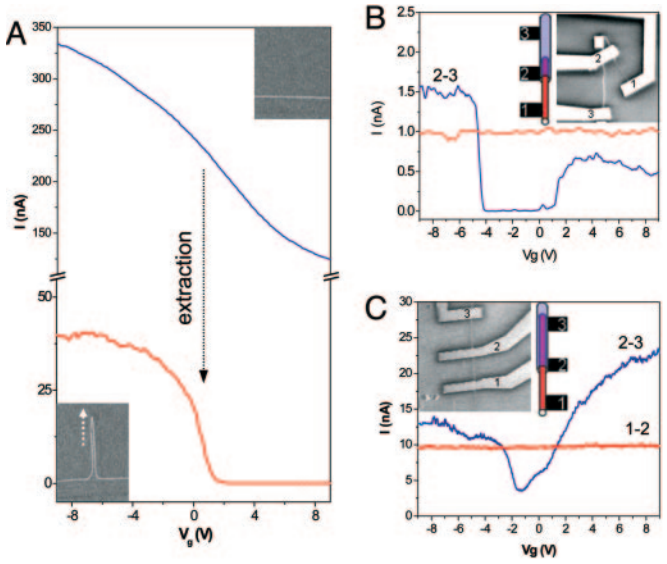

Fig. 3. SEM/AFM images and current–voltage characteristics of extracted nanotubes. (*A*) Plot of current as a function of gate voltage before (blue) and after (red) extraction. *Insets* show the structural change of the extracted MWNT. (*B* and *C*) Current–gate voltage plots of the final extracted nanotubes showing different electrical properties. The red and blue structures in the schematic represent metallic and semiconducting SWNTs, respectively. The numbers 1, 2, and 3 denote the electrodes. *Inset* in *B* represents the splitting of a double-walled carbon nanotube into segments of metallic [1–2] and semiconducting [2–3] SWNTs. The double-walled configuration in *B* [2–3] remains unchanged after extracting the metallic inner shell [1–2]. All measurements were performed at room temperature with $V_b = 45$ mV.

excitation used in the measurement, we assign this SWNT as having (5, 0) chiral indices (24).

Such small-diameter SWNTs have previously been reported as being formed within MWNT structures and the zeolite crystals (25, 26). The small diameter of these SWNTs can be understood in terms of stabilization induced by confinement of the outer shells or zeolite pores during the growth process. Growth of isolated SWNTs of such small diameter has not been achieved. In this study, we are able to obtain substantial lengths of these ultrathin SWNTs in an isolated form through the mechanical extraction process.

We characterized by atomic-force microscopy a large set of the innermost SWNTs prepared by the extraction technique. The measured AFM traces across the SWNTs exhibited apparent heights in the range of 0.7–1.3 nm. Because these heights correspond to distances determined by molecular forces, it is appropriate to interpret these values as including the atomic hard-wall radii. To approximate this effect, we consider the actual nanotube diameter to be 0.3 nm less than the value measured by atomic-force microscopy. Thus, the physical diameters of the extracted SWNTs range from $\approx$0.4 to 1.0 nm. We observed that $\approx$10% of the extracted SWNTs had diameters $<\approx$0.7 nm.

The electrical transport properties of extracted inner shells are expected to differ markedly from those of the parent MWNT, because the current is known to flow predominantly through a few outer shells (27). Such changes were indeed previously demonstrated in electrically induced shell-by-shell oxidation of MWNTs (8). We explored the electrical behavior by examining transport before and after extraction of the innermost SWNT from a pristine MWNT (Fig. 3*A*). The transport properties were analyzed by monitoring current I through the nanotube at a fixed bias voltage V_b as a function of the gate electric voltage (V_g). In the initial MWNT, the outermost metallic and semiconducting shells carry the current and produce a weak gate dependence of the conductance, presumably arising from a field effect in the outermost semiconducting shell. Upon extraction, the device characteristics change markedly. The overall conductance drops by an order of magnitude, and for the range of $V_g > 1$ V, the device is completely turned off. This result indicates that the current flows through semiconducting SWNTs for at least part of its path and can consequently be strongly modulated by the gate voltage V_g.

The fabrication of multiple electrodes in the extracted region of MWNTs allows the simultaneous investigation of intrashell and intershell transport. Fig. 3 *B* and *C* show two representative examples. In Fig. 3*B*, the final SWNT shell in the [1–2] segment displays metallic behavior (i.e., the current I is independent of gating voltage V_g). The [2–3] segment exhibits an ambipolar semiconducting behavior (28). This observation indicates that the final [1–2] SWNT shell is completely extracted from the [2–3] segment, leaving a hollow semiconducting SWNT in this region. In contrast, in Fig. 3*C*, the final [1–2] shell again shows metallic behavior, but the [2–3] segment exhibits a mixed semiconducting and metallic behavior, where I is suppressed but finite for all values of gate bias V_g. This result suggests that the [2–3] segment is a double-walled carbon nanotube with a metallic inner shell that is also present in the [1–2] region and is surrounded by a semiconducting outer shell that gives rise to the observed modulation of the conductivity.

The field-effect transport properties of extracted SWNTs of small diameter revealed a surprising result. Among the 20 extracted SWNT shells with diameters $<\approx$0.7 nm that were characterized at room temperature, none displayed transport behavior corresponding to a semiconductor with an appreciable band gap. Statistically, within the simple zone-folding picture of nanotube electronic structure, two-thirds of the SWNTs should be semiconductors. Thus, the experimental findings differ strongly from what would be expected for a random collection of larger-diameter nanotubes. The results may reflect the strong suppression of semiconducting band gaps due to the s-p hybridization for small-diameter SWNTs, such as the (5, 0) structure (29, 30). In addition, given the limited number of available SWNT structures of such small diameter, it is possible that fullerene-like end capping (26, 27) in the catalytic growth of MWNTs acts to favor production of innermost shells with chiral structures corresponding to metallic behavior.

Conclusion

We have demonstrated a simple but robust scheme for the controlled extraction of successive shells of MWNTs by means of a standard AFM. Engineering MWNTs by using manipulation with a standard AFM is able to demonstrate the following: The large-scale (up to a fraction of a millimeter) mechanical manipulation of ultralong MWNTs has enabled the successive extractions of inner shells down to subnanometer-diameter SWNTs with controlled patterns, without either electric vaporization or an oxidation procedure to remove the outer shells. The smallest individual SWNTs (as small as 0.4 nm) have been prepared as field-effect nanodevices. No other procedure has provided the isolated, high-quality, ultrathin SWNTs that we have achieved by using the present method. The method permits the creation of complex nanotube patterns, as well as the extraction of the innermost SWNTs. The innermost SWNTs can be isolated and have diameters as small as $\approx$0.4 nm. These features should permit many further studies of this important limiting class of ultrathin SWNTs. Interestingly, when prepared in field-effect test structures, these ultrathin SWNTs exhibit predominantly metallic electrical transport properties, in contrast to the expectations for a collection of larger-diameter tubes.

This work was supported by National Science Foundation (NSF) Award CHE-0117752; the New York State Office of Science, Technology, and Academic Research; the Creative Research Initiative of Korea Science and Engineering Foundation (KOSEF); and Brain Korea 21. B.H.H. was supported by the postdoctoral fellowship program of KOSEF. M.Y.S. was

supported by Department of Energy Basic Energy Sciences Grant FG02-98ER14861. P.K. was supported by the NSF Faculty Early Career Development Program (DMR-0349232) and the Defense Advanced Research Projects Agency (N00014-04-1-0591).

1. Iijima, S. (1991) *Nature* **354,** 56–58.
2. Yu, M.-F., Lourie, O., Dyer, M. J., Moloni, K., Kelly, T. F. & Ruoff, R. S. (2000) *Science* **287,** 637–640.
3. Fennimore, A. M., Yuzvinsky, T. D., Han, W.-Q., Fuhrer, M. S., Cumings, J. & Zettl, A. (2003) *Nature* **424,** 408–410.
4. Falvo, M. R., Clary, G. J., Taylor, R. M., Chi, V., Brooks, F. P., Washburn, S. & Superfine, R. (1997) *Nature* **389,** 582–584.
5. Wagner, H. D., Lourie, O., Feldman, Y. & Tenne, R. (1998) *Appl. Phys. Lett.* **72,** 188–190.
6. Ye, H., Lam, H., Titchenal, N., Gogotsi, Y. & Ko, F. (2004) *Appl. Phys. Lett.* **85,** 1775–1777.
7. Cumings, J. & Zettl, A. (2004) *Phys. Rev. Lett.* **93,** 086801.
8. Collins, P. G., Arnold, M. S. & Avouris, P. (2001) *Science* **292,** 706–709.
9. Kolmogorov, A. N. & Crespi, V. H. (2000) *Phys. Rev. Lett.* **85,** 4727–4730.
10. Kim, K. S., Tarakeshwar, P. & Lee, J. Y. (2000) *Chem. Rev.* **100,** 4145–4185.
11. Cumings, J. & Zettl, A. (2000) *Science* **289,** 602–604.
12. Cumings, J., Collins, P. G. & Zettl, A. (2000) *Nature* **406,** 586.
13. Zheng, Q. & Jiang, Q. (2002) *Phys. Rev. Lett.* **88,** 045503.
14. Sazonova, V., Yaish, Y., Üstünel, H., Roundy, D., Arias, T. A. & McEuen, P. L. (2004) *Nature* **431,** 284–287.
15. Ajayan, P. M., Ebbesen, T. W., Ichihashi, T., Iijima, S., Tanigaki, K. & Hiura, H. (1993) *Nature* **362,** 522–525.
16. Tsang, S. C., Harris, P. J. F. & Green, M. L. H. (1993) *Nature* **362,** 520–522.
17. Postma, H. W. Ch., Jonge, M. D., Yao, Z. & Dekker, C. (2000) *Phys. Rev. B* **62,** R10653–R10656.
18. Zheng, L. X., O'Connell, M. J., Doorn, S. K., Liao, X. Z., Zhao, Y. H., Akhadov, E. A., Hoffbauer, M. A., Roop, B. J., Jia, Q. X., Dye, R. C., *et al.* (2004) *Nat. Mater.* **3,** 673–676.
19. Ericson, L. M., Fan, H., Peng, H., Davis, V. A., Zhou, W., Sulpizio, J., Wang, Y., Booker, R., Vavro, J., Guthy, C., *et al.* (2004) *Science* **305,** 1447–1450.
20. Zhu, H. W., Xu, C. L., Wu, D. H., Wei, B. Q., Vajtai, R. & Ajayan, P. M. (2002) *Science* **296,** 884–886.
21. Hertel, T., Walkup, R. E. & Avouris, P. (1998) *Phys. Rev. B* **58,** 13870–13873.
22. Bachilo, S. M., Strano, M. S., Kittrell, C., Hauge, R. H., Smalley, R. E. & Weisman, R. B. (2002) *Science* **298,** 2361–2366.
23. Jorio, A., Pimenta, M. A., Filho, A. G. S., Saito, R., Dresselhaus, G. & Dresselhaus, M. S. (2003) *New J. Phys.* **5,** 139.1–139.17.
24. Li, I. L., Li, G. D., Liu, H. J., Chan, C. T. & Tang, Z. K. (2003) *Appl. Phys. Lett.* **82,** 1467–1469.
25. Qin, L.-C., Zhao, X., Hirahara, K., Miyamoto, Y., Ando, Y. & Iijima, S. (2000) *Nature* **408,** 50.
26. Wang, N., Tang, Z. K., Li, G. D. & Chen, J. S. (2000) *Nature* **408,** 50–51.
27. Bourlon, B., Miko, C., Forró, L., Glattli, D. C. & Bachtold, A. (2004) *Phys. Rev. Lett.* **93,** 176806.
28. Martel, R., Derycke, V., Lavoie, C., Appenzeller, J., Chan, K. K., Tersoff, J. & Avouris, P. (2001) *Phys. Rev. Lett.* **87,** 256805.
29. Machon, M., Reich, S., Thomsen, C., Sanchez-Portal, D. & Ordejon, P. (2002) *Phys. Rev. B* **66,** 155410.
30. Zólyomi, V & Kürti, J. (2004) *Phys. Rev. B* **70,** 085403.